



ELSEVIER

Contents lists available at ScienceDirect

Chinese Chemical Letters

journal homepage: [www.elsevier.com/locate/ccllet](http://www.elsevier.com/locate/ccllet)

## Three-dimensional heterogeneous electro-Fenton system with reduced graphene oxide based particle electrode for Acyclovir removal

Nan Cai<sup>a</sup>, Ge Bai<sup>a,b</sup>, Ting Zhang<sup>b</sup>, Yongqian Lei<sup>a</sup>, Pengran Guo<sup>a,\*</sup>, Zhiliang Chen<sup>c,\*</sup>, Jingwei Xu<sup>a</sup>

<sup>a</sup> Guangdong Provincial Key Laboratory of Chemical Measurement and Emergency Test Technology, Guangdong Provincial Engineering Research Center for Online Monitoring of Water Pollution, Institute of Analysis, Guangdong Academy of Sciences (China National Analytical Center, Guangzhou), Guangzhou 510070, China

<sup>b</sup> College of Petrochemical Engineering, Lanzhou University of Technology, Lanzhou 730000, China

<sup>c</sup> Guangdong Engineering Technology Research Center of Heavy Metal Pollution Control and Restoration in Farmland Soil, South China Institute of Environmental Sciences, MEE, Guangzhou 510535, China

### ARTICLE INFO

#### Article history:

Received 2 November 2022

Revised 3 April 2023

Accepted 25 April 2023

Available online 27 April 2023

#### Keywords:

Advanced oxidation

Three-dimensional electro-Fenton

Reduced graphene oxide

Acyclovir (ACV)

Degradation

### ABSTRACT

New pollutant pharmaceutical and personal care products (PPCPs), especially antiviral drugs, have received increasing attention not only due to their increase in usage after the outbreak of COVID-19 epidemics but also due to their adverse impacts on water ecological environment. Electro-Fenton technology is an effective method to remove PPCPs from water. Novel particle electrodes (MMT/rGO/Fe<sub>3</sub>O<sub>4</sub>) were synthesized by depositing Fe<sub>3</sub>O<sub>4</sub> nanoparticles on reduced graphene oxide modified montmorillonite and acted as catalysts to promote oxidation performance in a three-dimensional electro-Fenton (3D-EF) system. The electrodes combined the catalytic property of Fe<sub>3</sub>O<sub>4</sub>, hydrophilicity of montmorillonite and electrical conductivity of graphene oxides, and applied for the degradation of Acyclovir (ACV) with high efficiency and ease of operation. At optimal condition, the degradation rate of ACV reached 100% within 120 min, and the applicable pH range could be 3 to 11 in the 3D-EF system. The stability and reusability of MMT/rGO/Fe<sub>3</sub>O<sub>4</sub> particle electrodes were also studied, the removal rate of ACV remained at 92% after 10 cycles, which was just slightly lower than that of the first cycle. Potential degradation mechanisms were also proposed by methanol quenching tests and FT-ICR-MS.

© 2023 Published by Elsevier B.V. on behalf of Chinese Chemical Society and Institute of Materia Medica, Chinese Academy of Medical Sciences.

New pollutant pharmaceutical and personal care products (PPCPs) are receiving tremendous attention due to their potential threats to living organisms and human health [1–4]. The concentrations of PPCPs in the surface water and wastewater are from ng/L to µg/L [5,6]. PPCPs and their by-products, even at low doses, have adverse effects on non-target organs of human bodies or other organisms in the water ecosystem. Long-term presence of PPCPs in the environment may lead to adverse consequences [7,8]. Therefore, it is crucial to remove PPCPs from water ecological environment. PPCPs include all types of medications and daily personal care products. Among them, antiviral drugs are treatment drugs dangerous to aquatic organisms and induce environmental risks [9]. The outbreaks of COVID-19 epidemics rapidly increase antiviral drug usage leading to growing concern from the public [10].

Acyclovir (ACV) is one of the most widely used antiviral drugs to treat two common viral infections, chickenpox-zoster and herpes simplex [11–13], and it has been proposed for effective COVID-19 treatments [14]. ACV has low water solubility (2.5 mg/mL at 37 °C [15]) and poor absorption on the gastrointestinal tract due to its hydrophobicity, thus, it has short life span and low bioavailability (about 20%) [2] in human body. ACV and its by-products have been detected in surface water, drinking water, and wastewater treatment plant effluents [16–18], which indicate that ACV prescribed for treating viral infections can be easily found in aquatic environments [19]. Current water treatment technologies include adsorption, membrane purification, biological treatment, *etc.* However, the existing sewage treatment processes cannot completely degrade these antiviral drugs [12,20]. Adsorption and membrane purification can only achieve the enrichment of the drugs, not fully degrade of them. Plus, these techniques may produce hazardous wastes and their cost are relatively high. For biological treatment,

\* Corresponding authors.

E-mail addresses: [prguo@fenxi.com.cn](mailto:prguo@fenxi.com.cn) (P. Guo), [chenzhiliang@scies.org](mailto:chenzhiliang@scies.org) (Z. Chen).

the removal of such drugs with short life span is low efficient with poor stability. Therefore, it is necessary to seek new and efficient processes to remove ACV from the aquatic environment.

Recently, the electrochemical water treatment technique, as one of advanced oxidation processes (AOPs) [21] in which two-dimensional (2D) or three-dimensional (3D) electrode devices are applied, has attracted much attention because of its green, efficient and controllable characteristics [22–24]. Traditional 2D electrode system has some drawbacks such as serious corrosion of the electrode during operation, intractable electrode material replacement, high energy consumption, and high operation cost [25]. In 3D electrode system, particle electrodes are polarized under electrostatic induction forming numerous micro-electrodes, which can not only increase the specific surface area of electrodes, but also shorten the migration distance of reactants, and eventually improve current efficiency and treatment capacity [26]. However, most of these systems cannot achieve a substantial increase in catalytic efficiency, only with an increase of less than 30%. To improve degradation efficiency, it is necessary to explore new catalytic systems with higher catalytic property.

Electro-Fenton (EF) process normally employs ferrous active sites on solid catalysts for decomposition of  $H_2O_2$ . It would generate more  $\cdot OH$  and rapidly decompose organic contaminants than traditional Fenton process. Three-dimensional electro-Fenton (3D-EF) could combine the advantages of both EF and 3D electrode systems and greatly enhance water treatment efficiencies. The unique micro electrolysis zone formed by 3D system can facilitate Fe(II) regenerating on the surface of particle electrodes, which further promotes EF catalytic activity [27]. 3D-EF process may solve the problems such as the low production of oxidizing substances in 3D electrode system and the difficulty in recovering the catalysts in EF system. Hou *et al.* [28] built a new 3D-EF system using activated carbon derived from iron sludge (SAC-Fe) as a particle electrode to degrade nitrogen heterocyclic compounds (NHCs). The degradation rate can reach over 95% after 120 min. SAC-Fe acts as both particle electrodes and heterogeneous catalysts in the system, thus enhancing the oxidation activity. Meng *et al.* [26] degraded *p*-nitrophenol (*p*-NP) via building used a 3D-EF system with a synthesized new iron copper carbon black (Fe-Cu-C) composite as the particle electrode. The degradation rate could reach 88% after 6 h of continuous reaction. Therefore, catalytic particle electrode is the key factor in a 3D-EF system [29]. However, current research show that the catalytic particle electrodes have defects of corrosion resistance, specific surface areas, and stability. It is necessary to study and propose catalysts and particle electrodes with new materials and techniques.

Montmorillonite (MMT) is one of the most abundant natural clay minerals with 2D morphology and specific sandwich layer structure that includes a central octahedral layer ( $AlO_6$ ) and two tetrahedral layers ( $SiO_4$ ). MMT also has the advantages of large specific area, strong adsorption capacity, and low cost, so it has been considered as a green and promising catalyst support material [30]. However, the poor electrical conductivity of MMT would impede the electron transfer process. Graphene oxide (GO) is a unique 2D nanomaterial with high electrical conductivity, and it has been frequently used to improve electron transfer efficiency of composite catalysts [31]. GO can be reduced by thermal annealing or chemical treatment to yield a graphene derivative with lower oxygen content (rGO). GO and rGO have better dispersibility and a hydrophilic nature because of their structure and surface functional groups [32]. Therefore, surface modification of MMT with GO or rGO may greatly improve its properties in all respects.

Herein, we synthesized novel MMT/rGO/Fe<sub>3</sub>O<sub>4</sub> particle electrodes with Fe<sub>3</sub>O<sub>4</sub> nanoparticles depositing on reduced graphene oxide modified MMT (MMT/rGO/Fe<sub>3</sub>O<sub>4</sub>). Reduced graphene oxide, MMT and Fe<sub>3</sub>O<sub>4</sub> were integrated to construct the hierarchi-

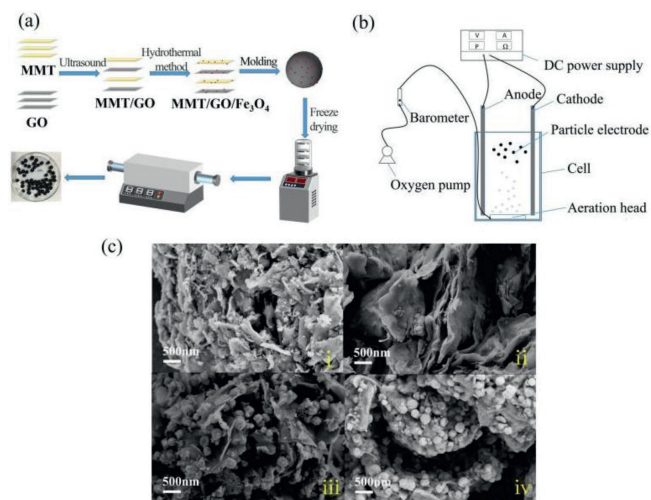


**Fig. 1.** MMT/rGO/Fe<sub>3</sub>O<sub>4</sub> particle electrodes synthesis procedures (a), the experimental setup of 3D-EF system (b), SEM images (c) (MMT (i), MMT/rGO (ii), MMT/Fe<sub>3</sub>O<sub>4</sub> (iii), MMT/rGO/Fe<sub>3</sub>O<sub>4</sub> (iv)).

cal ternary nanocomposites, which combined the catalytic property of Fe<sub>3</sub>O<sub>4</sub> [8], hydrophilicity of MMT and electrical conductivity of graphene. The electrocatalytic performances of the hierarchical ternary nanocomposites were investigated in a typical three-electrode system. The microstructure, morphology, and interfacial properties of the nanocomposites were characterized. The roles of nanomaterials in enhancing the catalytic performance were verified, and the molecular-level catalytic mechanisms of nanocomposites were also explored in a molecular level.

Figs. 1a and b showed the synthesis procedures of MMT/rGO/Fe<sub>3</sub>O<sub>4</sub> particle electrodes and the experimental setup of 3D-EF system, respectively. The detailed information were elaborated in Supporting Information. SEM images in Fig. 1c showed the morphology of MMT, MMT/rGO, MMT/Fe<sub>3</sub>O<sub>4</sub> and MMT/rGO/Fe<sub>3</sub>O<sub>4</sub>. The images revealed the layered structure of MMT with lots of fragments in 100–300 nm (Fig. 1c (i)), but those layers were further opened up in both MMT/rGO (Fig. 1c (ii)) and MMT/Fe<sub>3</sub>O<sub>4</sub> (Fig. 1c (iii)). The sheet-like layers became larger and more complete with much fewer fragments in MMT/rGO. Some of the layers were overlapped and the others were separated with a distance more than one micron. The distance provided enough space for the iron minerals deposited on the surfaces of the layers. Fig. 1c (iv) showed Fe<sub>3</sub>O<sub>4</sub> particles with more obvious and larger spherical structures in MMT/rGO/Fe<sub>3</sub>O<sub>4</sub> than in MMT/Fe<sub>3</sub>O<sub>4</sub>, with average diameter of 250 nm, which indicated the addition of reduced graphene oxide greatly promoted the deposition of Fe<sub>3</sub>O<sub>4</sub> molecules onto the more opened up layers in MMT/rGO. Therefore, the specific areas, the adsorption sites and the catalytic performance would be all enhanced greatly in the synthesized MMT/rGO/Fe<sub>3</sub>O<sub>4</sub> particle electrodes. Wide-survey XPS spectrum (Fig. S1b in Supporting information) and EDX analysis shown in Fig. S2 (Supporting information) also verified the coexistence of Fe, O, C, Si and Al. Although the composites had undergone repeated washing in water and ethanol by ultra-sonication before SEM, almost no isolated micro-spheres were observed outside the layered structure. This observation indicates strong chemical bonding has been formed between Fe<sub>3</sub>O<sub>4</sub> particles and the oxygen-bearing function groups in rGO [33]. The TEM image in Fig. S3 (Supporting information) further illustrated and verified the deposition of Fe<sub>3</sub>O<sub>4</sub> particles on the layers and their tightly connected structure. As shown in Table S1 (Supporting information), compared with MMT, the specific surface area of MMT/rGO/Fe<sub>3</sub>O<sub>4</sub> was nearly doubled, which explained that the interlayer structure of MMT

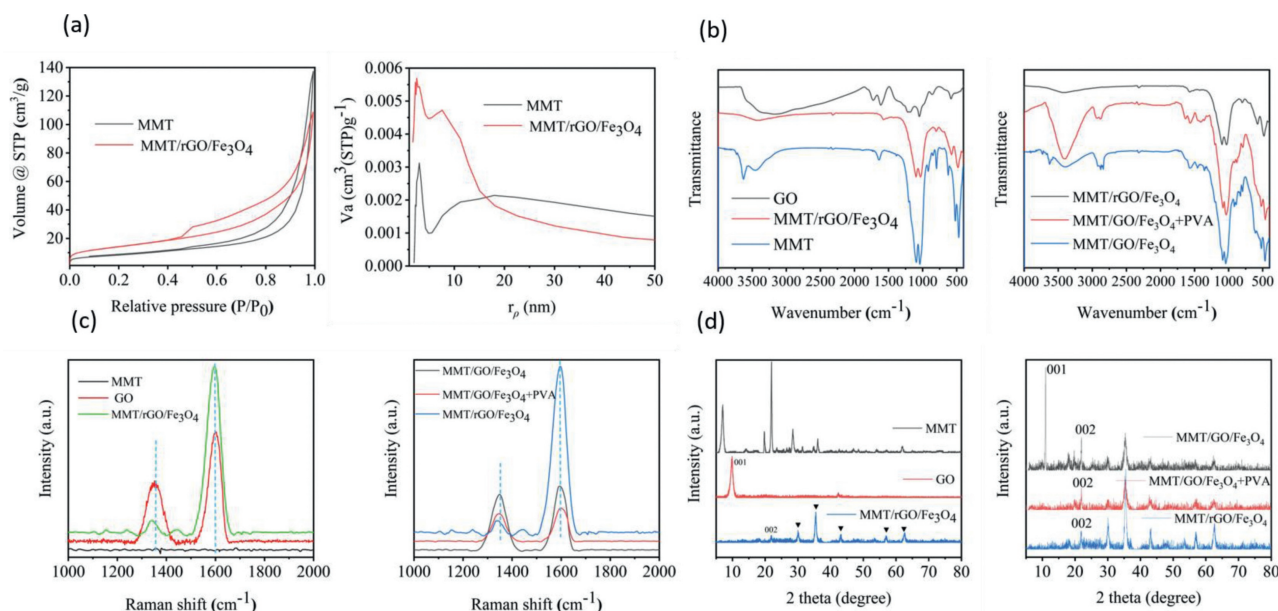


Fig. 2. The nitrogen adsorption-desorption curve and pore diameter distribution (a), FTIR spectra (b), Raman spectra (c), XRD patterns (d) of MMT and MMT/rGO/Fe<sub>3</sub>O<sub>4</sub>.

was opened widely and more voids were formed after loading with rGO and Fe<sub>3</sub>O<sub>4</sub>.

Fig. 2a illustrates the nitrogen adsorption-desorption curve and pore diameter distribution of MMT and MMT/rGO/Fe<sub>3</sub>O<sub>4</sub>. A typical type II isotherm and wide hysteresis area were observed and showed the wide distributions of pores in the composites. The porous structures in the materials were beneficial to adsorption and diffusion of pollutants on the catalysts. Pollutants in electrolyte could enter the pores in the catalysts and be adsorbed at the active sites to produce the intermediates in advanced oxidation. After that, the intermediates left the active sites and diffused away from the composite materials, which improve efficiency in the overall catalytic reactions.

The vibrational bands of the materials were studied by Fourier transform infrared spectroscopy (FTIR). Fig. 2b shows the peaks at 1040 cm<sup>-1</sup> and 469 cm<sup>-1</sup> were attributed to Si-O vibration of SiO<sub>4</sub> tetrahedron, representing Si-O-Si anti-symmetric vibration and bending vibration, respectively. The peaks at 3627, 3449, and 1639 cm<sup>-1</sup> were corresponding to the hydroxyl groups of Al-O-H and structural water. In the FTIR spectrum of MMT/rGO/Fe<sub>3</sub>O<sub>4</sub>, the bands of hydroxyl groups were weaker compared to that in MMT, presumably as a result of the formation of interfacial interaction via de-hydroxylation.

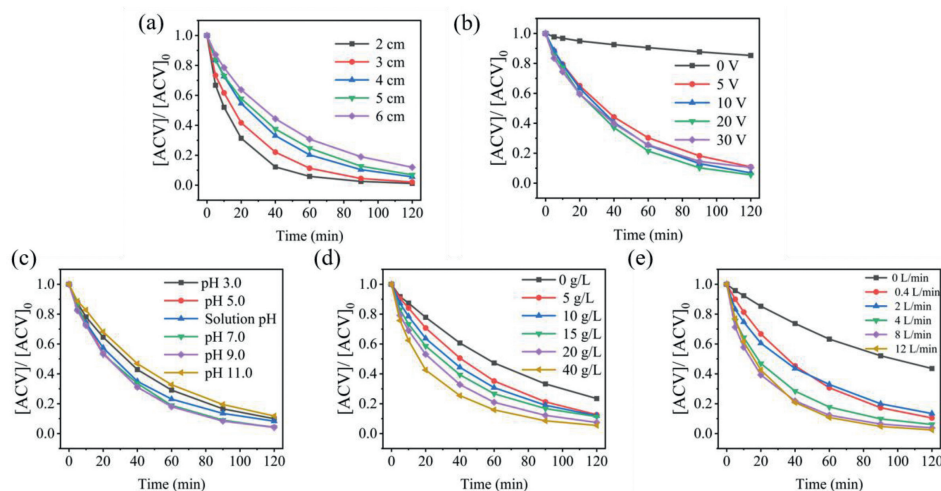
In Fig. 2c, the Raman spectra is applied to analyze the structural distortion of graphene in GO and MMT/rGO/Fe<sub>3</sub>O<sub>4</sub> composites. Two bands at around 1350 cm<sup>-1</sup> and 1600 cm<sup>-1</sup> were assigned to D-band and G-band, which were the out-plane oscillation of sp<sup>3</sup> defects and in-plane oscillation of sp<sup>2</sup> hybridization in hexagonal graphite structure. The intensity ratio of ID/IG decreased from 0.844 for GO to 0.836 for MMT/rGO/Fe<sub>3</sub>O<sub>4</sub>, indicating that the composite materials still have a strong order after calcination.

Fig. 2d shows XRD patterns of MMT, GO, MMT/rGO/Fe<sub>3</sub>O<sub>4</sub> and the products in the preparation process. A sharp diffraction peak (001) at about 10° was observed in the XRD spectra of GO. In the process of composite materials preparation, this strong characteristic peak gradually disappeared, but a new peak at 22° appeared corresponding to the (002) plane of graphite. This result indicated that GO was successfully reduced to graphene after hydrothermal process. The peaks at 30.0°, 35.4°, 43.0°, 53.3°, and 56.8° were as-

signed to (220), (311), (400), (511), and (440) crystal faces of Fe<sub>3</sub>O<sub>4</sub>, respectively. The (002) plane of graphite was also observed in the composites, which implied that GO was gradually reduced, and the amount of reduced GO gradually increased during the preparation process, and finally all of GO were reduced.

The electrode spacing in the electrochemical reaction system has a great influence on mass transfer rate. In order to investigate the effect of electrode spacing on the pollutant removal rate in the reaction system, the electrode spacing has been varied from 2 cm to 6 cm, and the degradation rate of ACV was calculated accordingly. Fig. 3a shows the effect of electrode spacing on ACV degradation rate in 3D-EF system with MMT/rGO/Fe<sub>3</sub>O<sub>4</sub> as particle electrodes. The electrode spacing was inversely proportional to ACV removal efficiency: the smaller the electrode spacing, the higher the removal rate. When the electrode distance was set from 2 cm to 6 cm, the removal efficiency is 99% to 92% after 120 min of reaction. As the distance between the plates was gradually decreased, the mass transfer distance was shortened, the side reaction rate becomes lower. Therefore, the degradation efficiency had been enhanced because the distance between the plates was shortened.

The applied voltage is a very important operation parameter to generate electric current and produce Fenton reagent, and it is also the main driving force of electrochemical reaction. Fig. 3b shows the effects of applied voltage, from 0V to 30V, on ACV degradation in 3D-EF system. The removal efficiency of ACV has been enhanced as the applied voltage increased from 0V to 20V, and then been impaired obviously as the applied voltage reach 30V. This might be because that the driving force of electro redox and the polarity of catalytic particle electrode are both enhanced as the increase of voltage [34]. The current density was also increased, which accelerated the formation of H<sub>2</sub>O<sub>2</sub> at the cathode, and finally promotes the decomposition of H<sub>2</sub>O<sub>2</sub> on the surface of particle electrodes to produce more •OH [35]. However, when the voltage further increased to 30V, the degradation rate would not continue to increase but decrease. As the applied voltage was getting higher, the current density was also getting larger, therefore, the side reactions would be invoked and intensified, such as hydrogen evolution reaction and oxygen evolution reaction (Eqs. 1-4). The side reactions could compete with the main reactions to degrade ACV, decrease



**Fig. 3.** Effect of electrode spacing (a), applied voltage (b), initial pH (c), catalyst dosage (d) and aeration intensity (e) on ACV degradation in 3D-EF reaction system. Experiment condition: initial ACV concentration 20 mg/L, electrolyte solution  $\text{Na}_2\text{SO}_4$  0.02 mol/L, reaction time 120 min.

the yield of  $\text{H}_2\text{O}_2$ , and ultimately lead to lowered degradation efficiency.



pH is one of the most important influencing factors in Fenton-like reactions, and it could affect multiple elementary processes in the electro-Fenton reactions. Fig. 3c shows the effect of initial pH changes on the degradation rate of ACV by MMT/rGO/ $\text{Fe}_3\text{O}_4$  in 3D-EF reaction system. When the solution pH is adjusted to 3.0 to 11.0, the removal rates of ACV is 88% to 96%, respectively. When pH varied, the discrepancy of the degradation efficiency of ACV was not obvious. The removal rates of ACV at pH of 5.0, 7.0, and 9.0 slightly increased, but decreased at pH 3.0 and 12.0. The results manifest that MMT/rGO/ $\text{Fe}_3\text{O}_4$  catalytic particle electrodes are suitable to be applied to water at a wide range of pH, which could overcome the problems of only low pH applicable in current Fenton system.

Particle electrodes have two main functions in a 3D-EF reaction system. One is as the third electrodes in the reaction, the other is as the catalysts. MMT/rGO/ $\text{Fe}_3\text{O}_4$  is used as both micro electrolytic cells and heterogeneous catalysts in 3D-EF system. Electrochemical impedance spectroscopy (EIS) curve in Fig. S4 (Supporting information) showed MMT/rGO/ $\text{Fe}_3\text{O}_4$  particle electrode has smaller semicircular diameter than MMT/ $\text{Fe}_3\text{O}_4$ , representing lowered electrochemical impedance to promote the electron transfer from the catalysts to the pollutants and therefore enhance ACV removal efficiency. After voltage is applied, the particle electrodes filled between the anode and cathode are repolarized into tiny electrolytic cells in an electric fields, therefore, they will greatly increase electrode areas in the electro-catalytic system, promote the migration of reactants, and eventually improve the current efficiency. In addition to the hydroxyl radicals generated in anode oxidation, the system fully utilized the active components in the particles as well as  $\text{H}_2\text{O}_2$  generated in the cathode to produce strong oxidizing hydroxyl radicals. Fig. 3d shows the effect of catalyst dosage on the degradation rate of ACV by MMT/rGO/ $\text{Fe}_3\text{O}_4$  in 3D-EF system. The efficiency of ACV removal increased with the increased dosage of catalytic particle electrodes. When the dosage was 0 g/L, the resid-

ual content of ACV was 20% after 120 min, which indicates that the removal rate of ACV by electro-Fenton system alone was only 80%. As the catalytic particles were introduced into the reaction system and the dosage was increased from 10 g/L to 40 g/L, the residual content of ACV is decreased from 12% to 5%. The improvement of removal efficiency may be due to the increase of specific surface areas and active binding sites of particle electrodes in the system, and the shortened mass transfer distance which could accelerate the production rate of  $\cdot\text{OH}$  and improve the degradation rate of pollutants adsorbed on the catalysts surface.

Dissolved oxygen is also a crucial factor in the electro-Fenton reaction process [36]. The electrons from the dissolved oxygen can react with water to produce hydrogen peroxide. In order to investigate the effect of dissolved oxygen on reaction rate, the aeration intensity in solution was varied as other reaction parameters were set unchanged. Fig. 3e shows the effect of aeration intensity on the degradation rate of ACV by MMT/rGO/ $\text{Fe}_3\text{O}_4$  in 3D-EF system. As shown in the figure, with the increase of aeration intensity, the efficacy of ACV removal has been significantly improved. ACV residual amount was 44% after 120 min reaction without any aeration, but the ACV residual amount directly reduced to 10% while the aeration intensity increased to 0.4 L/min to generate large bubbles in the reaction container. When the aeration intensity continued to increase to 12 L/min, fine bubbles are filled in the reaction container, and the catalytic particle electrodes move up and down violently. In this case, the remaining ACV amount decreased to only 2%. More than providing sufficient dissolved oxygen to the system, aeration can also enhance mass transfer and promote adsorption by increasing agitation in the solution.

According to the above experiments, optimum operating conditions of ACV removal by the 3D-EF reaction system were identified. To further verify the performance of MMT/rGO/ $\text{Fe}_3\text{O}_4$  magnetic particle electrodes, degradation experiments of ACV was carried out by 3D-EF and other systems for comparison. As shown in Fig. 4a, the concentration of ACV was kept unchanged after standing for 120 min, indicating that ACV solution is stable when exposed to the air. ACV adsorption by particle electrodes was also investigated. The results showed that adsorption only removed 12% ACV in 120 min, which was quite limited. In natural environment, contaminants could continuously exposed to dissolved oxygen. Therefore, it is necessary to exclude the influence of dissolved oxygen during the reaction processes. The removal rate of ACV was verified by aeration only, and ACV was only reduced by 3%, indicating that aeration has no direct effects on pollutant removal. Moreover,

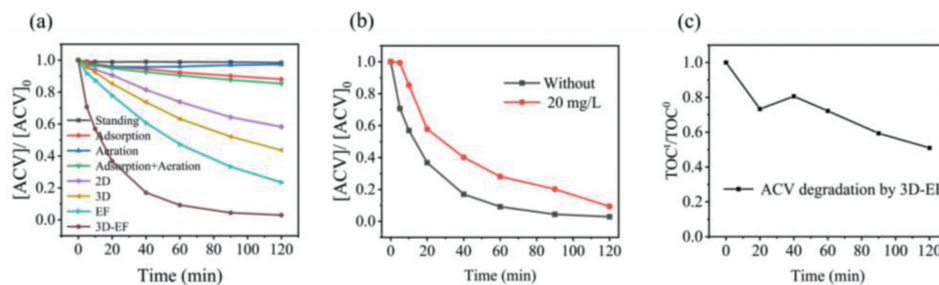


**Fig. 4.** Comparison of ACV degradation in different reaction systems (a), effect of dissolved organic matter (DOM) on the degradation rate of ACV in 3D-EF system (b), TOC removal efficiency of ACV in 3D-EF reaction system (c).

ACV removal rate with aeration and particle electrodes addition in the system were also examined without the assistance of electrochemical reaction. The results showed that ACV was reduced by only 15%, which equaled to the adding of ACV removal rate by aeration and adsorption alone. This indicated that there were no synergistic effects on ACV removal under the conditions of aeration and the particle electrodes addition in the reaction system. In 2D electrochemical system, only 42% ACV removal was achieved after 120 min. Meanwhile, using MMT/rGO/Fe<sub>3</sub>O<sub>4</sub> particle electrodes in 3D electrochemical system, the removal rate of ACV was 56%. For EF system, ACV removal rate was 77%. Low ACV removal efficiency in 2D system is due to the limited contact areas between the electrodes and the pollutants. The strong oxidizing substances generated were concentrated near the electrodes and could not fully react with the pollutants dispersing in the solution. The removal rate of ACV in 3D system is increased by 14% compared to that in 2D system. This is because that the particle electrodes in the solution formed tiny electrolytic cells, which strengthened the contact between pollutants and the oxidizing substances and sped up the mass transfer rate. Due to the very limited dissolved oxygen in the solution, direct oxidation on the anode in 2D system is the main way to degrade pollutants in the system, and the improvement of the removal rate is quite limited. The removal rate of ACV in EF process was 35% higher than that in 2D process, which is also higher than that in 3D process. This is because in EF process, dissolved oxygen in the solution increased. In addition to anodic oxidation and direct oxidation, strong oxidizing substances H<sub>2</sub>O<sub>2</sub> is also generated, and the amount of H<sub>2</sub>O<sub>2</sub> produced is proportional to the amount of dissolved oxygen in the solution.

In 3D-EF process, the removal rate of ACV was 97% after 120 min, which is 20% higher than that in EF process. This is because that electrostatic induction forms microelectrodes with opposite surface charges on the surface of MMT/rGO/Fe<sub>3</sub>O<sub>4</sub>. The electrochemical reaction would carry out on both the surface of the electrodes and the particle electrodes at the same time, so the reaction sites have been greatly increased and the efficiency of the direct and indirect electrolytic oxidation process has been improved. The 3D-EF oxidation process has synergistic effects: the EF process produces H<sub>2</sub>O<sub>2</sub> rapidly, and Fe<sub>3</sub>O<sub>4</sub> in the particle electrodes convert H<sub>2</sub>O<sub>2</sub> generated in the system into <sup>•</sup>OH, a stronger oxidant, resulting in much more efficient and rapid degradation of ACV.

In order to investigate the effect of dissolved organic matter (DOM) in the degradation rate of ACV in the reaction system, the experiments have been carried out with and without humic acid in the system. Fig. 4b shows the effect of humic acid on the degradation rate of ACV in 3D-EF system with MMT/rGO/Fe<sub>3</sub>O<sub>4</sub> as particle electrodes. When humic acid was present in the solution, it would compete with the target pollutants for degradation. As shown in Fig. 4b, the removal rate of ACV was reduced by 11% as humic acid existed. The results showed that the removal rate of target pollutants could be affected when other substances were existing in the solution but no obvious influences. Total organic carbon (TOC) was

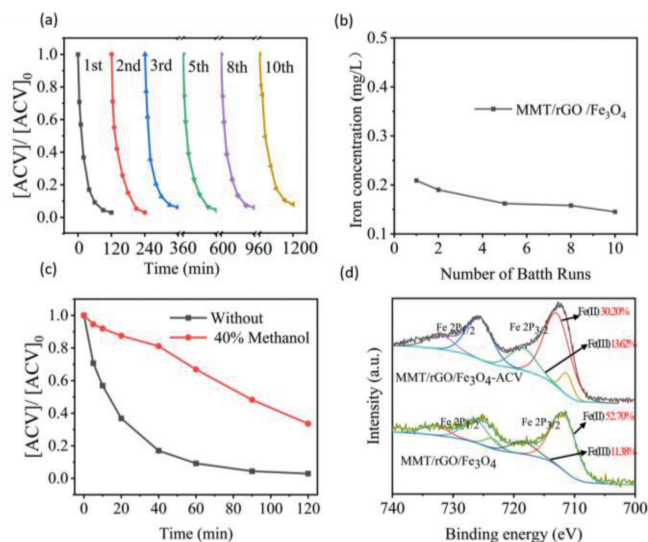


**Fig. 5.** Reusability after 10 cycles (a) and iron leaching (b) of MMT/rGO/Fe<sub>3</sub>O<sub>4</sub> in 3D-EF system, methanol quenching analysis in 3D-EF system (c), XPS spectra for Fe 2p regions of MMT/rGO/Fe<sub>3</sub>O<sub>4</sub> before and after reaction in 3D-EF system.

performed to access the mineralization of ACV and depicted in Fig. 4c. TOC removal rate achieved at 50% in 120 min, indicating the mineralization of ACV is not quite complete within 2 h. This may be attributed to the generated relatively stable small intermediate molecules during the degradation process, which reduced the mineralization efficiency.

Consecutive experiments have been performed to evaluate the stability and reusability of the MMT/rGO/Fe<sub>3</sub>O<sub>4</sub> particle electrodes. After each experiment cycle, the catalysts were recovered from the reaction solution by magnetic separation. They were rinsed repeatedly with deionized water and ethanol, and vacuum dried at 60 °C for subsequent tests. Iron leaching after each cycle was determined to evaluate the long-term stability of the MMT/rGO/Fe<sub>3</sub>O<sub>4</sub> particle electrodes. As shown in Figs. 5a and b, MMT/rGO/Fe<sub>3</sub>O<sub>4</sub> electrodes showed high activity even after 10 cycles, and the removal rate of ACV remained at 92%, which was just slightly lower than the first cycle. The precipitation of iron component from MMT/rGO/Fe<sub>3</sub>O<sub>4</sub> catalysis after reaction was 0.209–0.258 mg/L. After five cycles, the precipitation gradually stabilized at about 0.150 mg/L, and after eight cycles, the precipitation gradually stabilized at about 0.130 mg/L. This indicates that MMT/rGO/Fe<sub>3</sub>O<sub>4</sub> is very stable and can be reused. The slight decrease in the removal rate may be attributed to the repeated oxidation reaction on the active sites of iron in the particle electrodes or the incomplete removal of by-products in washing and drying processes, which might reduce the active sites of the catalysts and indirectly affect the degradation of ACV [37]. The stability of the MMT/rGO/Fe<sub>3</sub>O<sub>4</sub> particle electrodes was verified by comparing the XRD patterns of

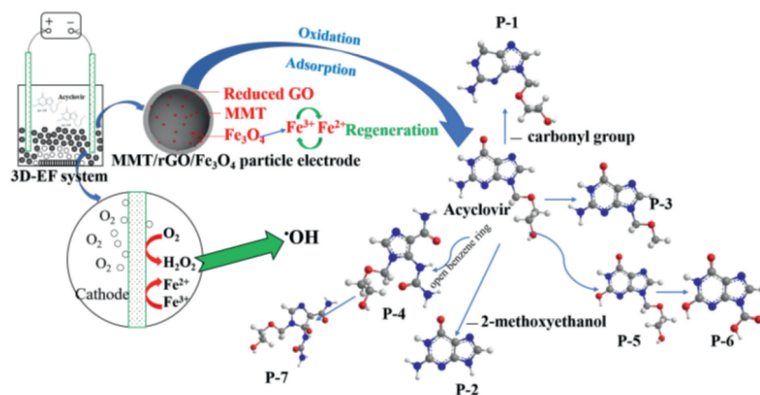


Fig. 6. The possible catalytic mechanism of ACV degradation by 3D-EF system.

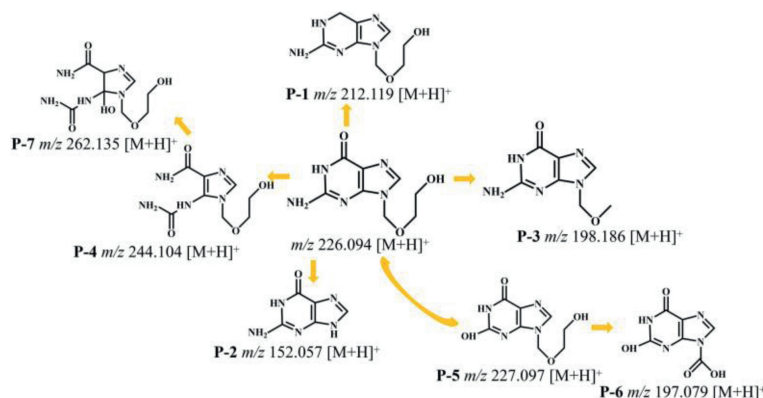


Fig. 7. The possible degradation pathways of ACV by 3D-EF system.

MMT/rGO/Fe<sub>3</sub>O<sub>4</sub> composites before and after reaction. The sharp characteristic peaks of 30.0°, 35.4°, 43.0°, 53.3°, and 56.8° which assigned to the crystal faces of Fe<sub>3</sub>O<sub>4</sub> could still be observed obviously after the heterogeneous catalysis (Fig. S1a), which indicates that the structure of the material has not changed before and after the reaction. The reduction of its strength might be caused by the loss of some iron, which was also consistent with the change of iron concentration (Fig. 5b) in the reaction process.

To further explore the degradation mechanisms of ACV by 3D-EF system, methanol quenching tests were performed. The objects that could be quenched by methanol in this reaction system are H<sub>2</sub>O<sub>2</sub> and  $\cdot OH$ . As shown in Fig. 5c, after adding 40% anhydrous methanol, the removal rate of ACV decreased by 30.6% after 120 min. The results showed that the contribution percentage of H<sub>2</sub>O<sub>2</sub> and  $\cdot OH$  in the ACV degradation process by 3D-EF system with MMT/rGO/Fe<sub>3</sub>O<sub>4</sub> as particle electrodes was about 30.6%, indicating that the degradation of ACV by H<sub>2</sub>O<sub>2</sub> and  $\cdot OH$  is not the main degradation pathway, and there are other removal pathways.

The possible mechanisms for ACV degradation on 3D heterogeneous EF system is discussed. The oxygen in the solution diffused on the surface of cathode to form H<sub>2</sub>O<sub>2</sub>. Then, H<sub>2</sub>O<sub>2</sub> reacts with ferrous sites in MMT/rGO/Fe<sub>3</sub>O<sub>4</sub> composite to form  $\cdot OH$  [38]. ACV molecules were attacked by the strong oxidant. During the reaction, the ferrous ions were also transformed into ferric ions [39]. Meanwhile, the electron transfer on micro electrodes reduces ferric iron again to ferrous iron, which enable a sufficient number of ferrous active sites for the heterogeneous reactions. As shown in Fig. 5d, XPS was used to characterize the catalysts MMT/rGO/Fe<sub>3</sub>O<sub>4</sub> before and after reaction. By comparing the ratio of Fe(II)/Fe(III), we found that the ratio increased from 0.216 (before reaction) to 0.302 (after reaction). The 40% increase of Fe(II)/Fe(III) ratio may be at-

tributed to the reduction of Fe(III) during the electro-catalysis process. The generated Fe(II) plays a very important role in the heterogeneous electro-Fenton reaction [40]. The catalytic mechanism was described in Fig. 6.

The oxidative mineralization intermediate products of ACV by advanced oxidation processes have been discussed by many researchers [41–43], to identify the intermediate products of ACV degradation by 3D-EF system FT-ICR-MS was employed. The detected degradation products were product P-1 to product P-7 with a proposed degradation pathway (Fig. 7) [19]. The oxidizing agents  $\cdot OH$  activated by catalysis attacked the benzene ring, the carbonyl bond, C–C and C–N bonds. The most abundant immediate product is P-2 with *m/z* 152.057, which may represent the species of protonated guanine that has also been reported by other researchers [21,44]. P-2 is produced by removing the 2-methoxyethanol (74 Da) side chain from ACV [45,46]. The intermediate firstly found in our research is P-1 with *m/z* 212.119, which is obtained by removing the carbonyl group from ACV.

In conclusion, the novel particle electrodes, MMT/rGO/Fe<sub>3</sub>O<sub>4</sub>, were synthesized by depositing Fe<sub>3</sub>O<sub>4</sub> nano-particles on reduced graphene oxide modified montmorillonite in this study. The microstructure, morphology, and interfacial property of the nanocomposites were characterized. The electro-catalytic performance of obtained particle electrodes were also investigated in a typical 3D-EF system. This 3D-EF system exhibited great degradation efficiency of ACV, and the degradation rate could reach 100% in 120 min under optimal conditions. The applicable pH range of the catalytic particle electrodes was in 3–11. The stability and reusability of MMT/rGO/Fe<sub>3</sub>O<sub>4</sub> particle electrodes were also studied, and the experiments showed that after 10 cycles, the removal rate of ACV stayed at 92%, which was just slightly lower than that of the

first cycle. The degradation of ACV by H<sub>2</sub>O<sub>2</sub> and ·OH is not the main degradation pathway and possible mechanism for ACV degradation were proposed.

### Declaration of competing interest

The authors declare that they have no known competing financial interests or personal relationships that could have appeared to influence the work reported in this paper.

### Acknowledgments

The study was financially supported by the GDAS' Project of Science and Technology Development (No. 2020GDASYL-20200103044), Key-Area Research and Development Program of Guangdong (No. 2020B1111350002), the National Key R&D Program of China (No. 2019YFC1805305), the Project of Water Resource Department of Guangdong Province (No. 2017-18).

### Supplementary materials

Supplementary material associated with this article can be found, in the online version, at doi:10.1016/j.ccl.2023.108514.

### References

- [1] R.Y. Krishnan, S. Manikandan, R. Subbaiya, et al., *Environ. Technol. Inno.* 23 (2021) 101757.
- [2] M.S. Gurgel Assis, T.C. Fernandes Pedrosa, F.S. de Moraes, et al., *J. Pharm. Sci.* 110 (2021) 1557–1571.
- [3] M.M. Yu, H.X. Li, J.Y. Xie, Y. Xu, X.Q. Lu, *Talanta* 236 (2022) 122875.
- [4] Z.H. Diao, S.T. Huang, X. Chen, et al., *J. Clean. Prod.* 330 (2022) 129806.
- [5] Y. Xiang, H.H. Wu, L. Li, et al., *Ecotox. Environ. Saf.* 213 (2021) 112044.
- [6] T. Wang, J. He, J. Lu, et al., *Chin. Chem. Lett.* 32 (2022) 3585–3593.
- [7] C.Z. Zhou, J.W. Chen, Q. Xie, et al., *Chemosphere* 138 (2015) 792–797.
- [8] H.S. Zheng, Y.Y. Hou, S. Li, et al., *Chin. Chem. Lett.* 33 (2022) 5013–5022.
- [9] H. Sanderson, D.J. Johnson, T. Reitsma, et al., *Regul. Toxicol. Pharm.* 39 (2004) 158–183.
- [10] L. Yao, W.Y. Dou, Y.F. Ma, Y.S. Liu, *Chemosphere* 282 (2021) 131047.
- [11] D. Russo, A. Siciliano, M. Guida, et al., *Water Res.* 122 (2017) 591–602.
- [12] A. Gupta, R.K. Vyas, A.B. Gupta, *J. Water Process Eng.* 39 (2021) 101855.
- [13] T. Oka, M. Hishizawa, K. Yamashita, K. Shiraki, A. Takaori-Kondo, *J. Infect. Chemother.* 27 (2021) 755–758.
- [14] M. Babu Singh, P. Jain, J. Tomar, et al., *J. Indian Chem. Soc.* 99 (2022) 100433.
- [15] J. Wadhawan, P.K. Parmar, A.K. Bansal, *J. Drug Deliv. Sci. Technol.* 65 (2021) 102662.
- [16] X.Z. Peng, C.Q. Wang, K. Zhang, et al., *Sci. Total. Environ.* 466–467 (2014) 755–761.
- [17] P.M. Bradley, L.B. Barber, J.W. Duris, et al., *Environ. Pollut.* 193 (2014) 173–180.
- [18] I. Pugajeva, L.E. Ikkere, M. Jansons, et al., *J. Pharm. Biomed. Anal.* 205 (2021) 114295.
- [19] T.C. An, J.B. An, Y.P. Gao, et al., *App. Catal. B: Environ.* 164 (2015) 279–287.
- [20] M.C. Yu, H.J. Liang, R.N. Zhan, L. Xu, J.F. Niu, *Chin. Chem. Lett.* 32 (2021) 2155–2158.
- [21] C. Liu, Y.P. Wang, Y.T. Zhang, et al., *Chem. Eng. J.* 354 (2018) 835–848.
- [22] J. Gimenez, B. Bayarri, Ó. González, S. Malato, S. Esplugas, *ACS Sustain. Chem. Eng.* 3 (2015) 3188–3196.
- [23] O. Nihal, Z.Hui H.D.Eric, et al., *Environ. Sci. Technol.* 49 (2015) 12187–12196.
- [24] L. Xu, X.Y. Cui, J.B. Liao, et al., *Chin. Chem. Lett.* 33 (2022) 3701–3704.
- [25] Y. Hu, F.Z. Yu, Z.T. Bai, et al., *Chemosphere* 308 (2022) 136544.
- [26] X.Z. Meng, K. Li, Z.K. Zhao, et al., *Sep. Purif. Technol.* 298 (2022) 121672.
- [27] M. Hajiahmadi, M. Zarei, A. Khataee, *J. Ind. Eng. Chem.* 96 (2021) 254–268.
- [28] B.L. Hou, B.Z. Ren, R.J. Deng, et al., *RSC Adv.* 7 (2017) 15455–15462.
- [29] W.Q. Sun, Y.J. Sun, K.J. Shah, P.C. Chiang, H.L. Zheng, *J. Hazard. Mater.* 370 (2019) 24–32.
- [30] N.P. Shetti, D.S. Nayak, S.J. Malode, R.M. Kulkarni, *Sens. Biosens. Res.* 14 (2017) 39–46.
- [31] D.W. Lee, L. De Los Santos V, J.W. Seo, et al., *J. Phys. Chem. B* 114 (2010) 5723–5728.
- [32] M.I. Tayouri, S. Estaji, S.R. Mousavi, et al., *Polym. Degrad. Stabil.* 206 (2022) 110179.
- [33] F. He, J.T. Fan, D. Ma, et al., *Carbon* 48 (2010) 3139–3144.
- [34] H.H. Phan Quang, T.P. Nguyen, D.D. Duc Nguyen, et al., *Chemosphere* 297 (2022) 134074.
- [35] H. Pourzamani, Y. Hajizadeh, N. Mengelizadeh, *Process Saf. Environ. Prot.* 119 (2018) 271–284.
- [36] L. Tian, Q.F. Zhuo, J.C. Lu, et al., *Chin. Chem. Lett.* 33 (2022) 4740–4745.
- [37] Z.D. Fang, K. Zhang, J. Liu, J.Y. Fan, Z.Q. Zhao, *Water Sci. Eng.* 10 (2017) 326–333.
- [38] Y.M. Zhang, Z. Chen, P.P. Wu, et al., *J. Hazard. Mater.* 393 (2020) 120448.
- [39] H.S. Zheng, Y.Y. Hou, S. Li, et al., *Chin. Chem. Lett.* 34 (2023) 107253.
- [40] H. Ghanbarlou, B. Nasernejad, M.N. Fini, M.E. Simonsen, *J. Muff. Chem. Eng. J.* 395 (2020) 125025.
- [41] G. Knopp, C. Prasse, T.A. Ternes, P. Cornel, *Water Res.* 100 (2016) 580–592.
- [42] L. Schlüter Vorberg, C. Prasse, T.A. Ternes, H. Mückter, A. Coors, *Environ. Sci. Technol. Lett.* 2 (2015) 342–346.
- [43] C. Prasse, M. Wagner, R. Schulz, T.A. Ternes, *Environ. Sci. Technol.* 45 (2011) 2761–2769.
- [44] G.Y. Li, X. Nie, Y.P. Gao, T.C. An, *App. Catal. B: Environ.* 180 (2016) 726–732.
- [45] J.J. Sasanya, A.M.M. Abd-Alla, A.G. Parker, A. Cannavan, *J. Chromatogr. B* 878 (2010) 2384–2390.
- [46] M. Yadav, V. Upadhyay, P. Singhal, S. Goswami, P.S. Shrivastav, *J. Chromatogr. B* 877 (2009) 680–688.